Acta Crystallographica Section B
Structural Science
ISSN 0108-7681

Experimental charge-density study on the nickel(II) coordination complex $[Ni(H_3L)][NO_3][PF_6]$ [H_3L = *N*,*N*′,*N*″-tris(2-hydroxy-3-methylbutyl)-1,4,7-triazacyclononane]: a reappraisal

L. J. Farrugia,[a]* C. S. Frampton,[a] J. A. K. Howard,[b] P. R. Mallinson,[a] R. D. Peacock,[a] G. T. Smith[a] and B. Stewart[b]

[a]WestCHEM, Department of Chemistry, University of Glasgow, Glasgow G12 8QQ, Scotland, and [b]Department of Chemistry, University of Durham, Durham DH1 3LE, England

Correspondence e-mail: louis@chem.gla.ac.uk

Received 11 October 2005
Accepted 6 January 2006

The experimental charge density in the title complex has been re-examined. The original work, reported some 8 years ago [Smith *et al.* (1997). *J. Am. Chem. Soc.* **119**, 5028–5034], was undertaken using a very early version of the *XD* software, which contained serious programming errors. A re-refinement, using the original data and a recent version of the *XD* software, shows that many of the unusual aspects of this earlier study are artefacts due to these programming errors. The topological properties of the newly obtained experimental density compare well with those calculated from a theoretical DFT (density-functional theory) UHF-SCF (unrestricted Hartree Fock–self-consistent field) density. This report corrects several erroneous conclusions regarding the charge density in the title complex – in particular, the highly unusual diffuse Laplacian distribution about the Ni atom, and the trifurcated bond path from the Ni atom to the alcohol oxygen donor atoms are no longer observed. An examination of a range of topological properties of the metal–ligand bonds leads to the conclusion that the Ni—N and Ni—O bonds have an intermediate character, with a significant shared interaction, but with a substantial ionic component. This new study also reveals a previously unrecognized intramolecular H···H interaction in the macrocyclic ligand.

1. Introduction

Some 8 years ago we reported (Smith *et al.*, 1997) one of the first experimental charge density studies on a transition metal compound that utilized the topological AIM methodology of Bader (1990). This study, on the pendant-arm macrocyclic nickel(II) coordination complex $[Ni(H_3L)][NO_3][PF_6]$ (1) with the ligand H_3L = *N*,*N*′,*N*″-tris(2-hydroxy-3-methyl butyl)-1,4,7-triazacyclononane [see (I); Fallis *et al.*, 1993], showed a number of features, which with hindsight appeared quite puzzling. These included:

(i) highly unusual features in the Laplacian about the Ni centre, which we attributed to diffuse sp^3 density,

(ii) an unprecedented trifurcated bond path from the Ni atom towards the three alcohol oxygen donor atoms and

(iii) extremely high values of $\rho(\mathbf{r}_b)$ at the bond critical points (BCPs) for the Ni—O and especially for the Ni—N bonds [0.93 (4) and 3.10 (6) e Å^{-3}, respectively].

The X-ray diffraction data were analysed using a very early version of the *XD* software (Koritsanszky *et al.*, 1995), which has subsequently been significantly modified and upgraded (Koritsanszky *et al.*, 2003). After our study was published, a major coding error was discovered in the early version of *XD*, which involved an incorrect κ' scaling (κ' used rather than κ'^3) in the calculation of the density by the program *XDPROP*

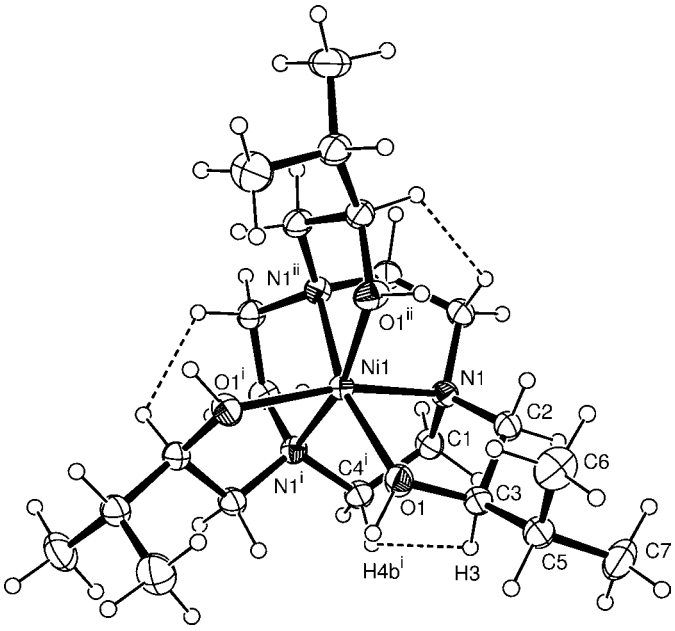

Figure 1
Displacement ellipsoid plot of the cation of (1), drawn at the 80% probability level, showing the atomic labelling scheme. Primed atoms indicated by (i) and (ii) are related to unprimed atoms by the symmetry operations z, x, y and y, z, x, respectively.

(Koritsanszky *et al.*, 2003). This affected all atomic centres, but was most important when the κ' value differed significantly from 1.0, as was the case for the Ni atom. This coding error was discovered in 1997 and corrected before the 1999 release of the program (*Rev*-14), but it seriously affected our original study, resulting in a substantially incorrect valence density around this atom, and a frankly bizarre appearance to the Laplacian. Other coding errors in *XD* affecting transition metals have subsequently been reported in the literature (Macchi *et al.*, 1998, 2002; Tafipolsky *et al.*, 2002; Macchi & Sironi, 2003; Scherer & McGrady, 2004) and have been corrected with the release of *XD* Version 4.9 in 2003 (Koritsanszky *et al.*, 2003). Full details of these coding errors are given in the supplementary material.[1]

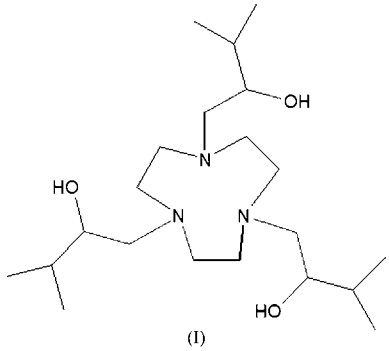

(I)

[1] Supplementary data for this paper are available from the IUCr electronic archives (Reference: BS5024). Services for accessing these data are described at the back of the journal.

Table 1
Experimental details.

Crystal data	
Chemical formula	$C_{21}H_{45}N_3NiO_3{\cdot}F_6P{\cdot}NO_3$
M_r	653.29
Cell setting, space group	Cubic, $P2_13$
a (Å)	14.008 (2)
V (Å^3)	2748.7 (7)
Z	4
D_x (Mg m^{-3})	1.579
Radiation type	Mo $K\alpha$
No. of reflections for cell parameters	25
θ range (°)	2–23
μ (mm^{-1})	0.85
Temperature (K)	123 (2)
Crystal form, colour	Octahedron, dark blue
Crystal size (mm)	0.6 × 0.4 × 0.4
Data collection	
Diffractometer	Enraf–Nonius CAD4
Data collection method	Profile-fitted $\theta/2\theta$ scan
Absorption correction	Gaussian
T_{min}	0.774
T_{max}	0.804
No. of measured, independent and observed reflections	20 445, 6017, 5095
Criterion for observed reflections	$I > 2\sigma(I)$
R_{int}	0.017
θ_{max} (°)	49.9
Range of h, k, l	$1 \Rightarrow h \Rightarrow 30$ $0 \Rightarrow k \Rightarrow 30$ $-17 \Rightarrow l \Rightarrow 10$
No. and frequency of standard reflections	5 every 120 min
Intensity decay (%)	0.5
Refinement	
Refinement on	F
$R[F^2 > 2\sigma(F^2)]$, $wR(F^2)$, S	0.0219, 0.0152, 1.06
No. of reflections	5095
No. of parameters	354
H-atom treatment	Mixture of independent and constrained refinement
Weighting scheme	$w_1 = 1/[\sigma^2(F_o)]$
$(\Delta/\sigma)_{max}$	<0.0001
$\Delta\rho_{max}$, $\Delta\rho_{min}$ (e Å^{-3})	0.28, −0.24
Extinction method	Becker–Coppens type 1 Lorentzian isotropic
Extinction coefficient	0.67 (5)

Computer programs used: *CAD*4 software (Enraf–Nonius, 1994), *DREAR* (Blessing, 1987), *SHELXS* (Sheldrick, 1993), *XD* (Koritsanszky *et al.*, 2003), *ORTEP*3 for Windows (Farrugia, 1997).

In view of these problems, and in light of subsequent experimental charge density studies on nickel(II) and cobalt(II) coordination compounds (Iversen *et al.*, 1997; Hwang & Wang, 1998; Lee *et al.*, 1999, 2002; Ptasiewicz-Bak *et al.*, 1999; Kožíšek *et al.*, 2004), which showed very different features, we decided to re-investigate the charge density in complex (1), using a recent release of the *XD* software (Version 4.10). This version of *XD* has been shown in a number of studies (Lee *et al.*, 2002; Macchi *et al.*, 2001, 2002; Macchi & Sironi, 2003; Farrugia *et al.*, 2003; Farrugia & Evans, 2005) to provide reliable charge densities from experimental data on transition metal complexes that are in good agreement with the densities from accurate quantum calculations. Our revised interpretation of the charge density in (1) is based on

re-refinements using the original diffraction data (Smith *et al.*, 1997) and is undertaken in the light of developments that have taken place since our original report. As well as reappraising the experimental data, we also now include theoretical DFT(B3LYP) UHF-SCF calculations, which support our revised interpretations. This paper should be regarded as a correction for our previous reports (Smith *et al.*, 1996, 1997) on the charge density in (1). The original reasons for choosing this study remain valid: it represents a challenge for the charge-density method, since the non-centrosymmetric chiral complex has C_3 symmetry, with tertiary amine N and alcohol O donors. The latter could potentially bind as a pure σ donor, formally using one lone pair, or as a σ–π donor formally using two lone pairs.

2. Experimental procedures

Details of the data collection and data treatment were reported previously (Smith *et al.*, 1996, 1997) and are given in Table 1. An *ORTEP* plot of the complex cation is shown in Fig. 1. The cation and the NO_3^- and PF_6^- anions are all ordered and lie along the crystallographic threefold axis. Many of the difficulties in refinement, which we originally described (Smith *et al.*, 1997), such as unrealistic values of the thermal parameters and absences of expected bond paths, were not encountered in this present study. Nevertheless, complex (1) crystallizes in a non-centrosymmetric, high-symmetry space group and problems with the least-squares refinement could be anticipated in view of previous work (El Haouzi *et al.*, 1996; Pérès *et al.*, 1999). The multipole formalism (Hansen & Coppens, 1978) as implemented in the *XD* program suite (Koritsanszky *et al.*, 2003) was used, and the function minimized in the least-squares procedure was $\Sigma w(|F_o| - k|F_c|)^2$. We took the opportunity to examine a number of models, including the one which we originally published where both of the $l = 0$ multipoles P_v and P_{00} were refined. This model, using radial functions which were essentially the same as those described below for the final model, converged to give reasonably similar parameter values only if the multipoles and their associated expansion–contraction parameters κ' were refined in separate blocks. If both sets of parameters were refined in the same block, physically unrealistic and highly negative populations for P_{00} were obtained. It became clear that, in this case at least, refinement of both the P_v and P_{00} multipoles was unnecessary and unprofitable. With data obtained at much lower temperatures, it may prove profitable to pursue a more extensive multipole model for the transition metal, *e.g.* as has been found for the nickel(II) centre in *trans*-$[Ni(NH_3)_4(NO_2)_2]$ (Iversen *et al.*, 1997). While most of our models converged without trouble, we found that many gave a virtually identical fit and were difficult to distinguish between on a statistical basis, as has been previously noted (Pérès *et al.*, 1999) for non-centrosymmetric structures.

The final refinement used only those reflections with $I > 2\sigma(I)$. Parameters were refined in blocks to avoid correlations. Initially all positional and displacement parameters were refined in one block, all multipole populations in another block, and the κ and κ' parameters in a third block. In a final block, all the parameters except the H-atom displacement parameters, and the κ and κ' parameters were co-refined to provide the least-squares estimates of errors. These cycles were repeated until convergence. The multipole expansion was truncated at the hexadecapole level for the Ni and P atom, and at the octupole level for all other non-H atoms. Each non-H pseudoatom was assigned a core and spherical-valence scattering factor constructed from the relativistic Dirac–Fock wavefunctions (Su & Coppens, 1998) expanded in terms of the single ζ functions (Bunge *et al.*, 1993). The radial fit of the spherical valence density was optimized by refinement of the expansion–contraction parameter κ. For the Ni atom, the radial terms for the valence deformation functions were single ζ Slater-type radial functions (for $l = 0$, 1, 3) or the relevant order Fourier–Bessel transforms of the wavefunctions (Su & Coppens, 1998; for $l = 2$, 4). For other atoms the radial terms were single ζ Slater-type radial functions. For all pseudo atoms, the valence-deformation radial fits were optimized by refinement of their expansion–contraction parameters κ', although for the P atom this proved problematical and the value of this parameter was fixed at 1.0. For the H atoms, only a monopole and bond-directed dipole were used, with the κ and κ' parameters fixed at 1.2. The C—H bond vectors were re-normalized to 1.083 Å and the O—H vector to 1.0 Å. The monopole populations of H atoms attached to the same carbon were constrained to be identical. The initial charge on the NO_3^- and PF_6^- anions was set to 1.0 and kept fixed during refinement, while maintaining overall electro-neutrality for the asymmetric unit. The monopole populations of the two independent F atoms were constrained to be identical. In our original study, the doubly charged ionic scattering factor for Ni was used and we examined the use of both the neutral atom and the Ni^{2+} scattering factor. The difference between the two is only significant for $\sin\theta/\lambda < 0.2$ and only some 50 reflections are sensitive to this difference. In refinements using either all the data with $I > 2\sigma(I)$ or only those data with $\sin\theta/\lambda < 0.2$, the two models gave virtually identical indices of fit. In the absence of convincing evidence either way, the neutral atom scattering factor was applied in the final model. We therefore conclude that it is not possible to determine the population of diffuse 4*s* density from the experimental diffraction data and in this model the 4*s* population on Ni is fixed at 2.0 and is not varied.

An adequate deconvolution of the thermal motion from the bonding density was judged from the rigid-bond criterion (Hirshfeld, 1976). The mean and largest Δ-m.s.d.a. (mean square displacement amplitudes) values were 8 and 21 $\times$ 10^{-4} Å^2, respectively, with the largest value for Ni—O1. Final residual maps calculated using the full data set were similar to those we originally reported, with a peak of 0.475 e Å^{-3} at the Ni centre. It appears that these residuals arise from the very highest angle data, since a map calculated using only those data with $\sin\theta/\lambda \leq 1.0$ is virtually featureless. It is possible that the high-angle data for (1), which were collected using a serial detector, suffer from scan-truncation errors (Destro & Marsh,

Table 2
CP properties for H_3L and anions.

The first line gives the experimental values and the second line the theoretical values (not available for the anion bonds).

	Length (Å)	$\rho(\mathbf{r}_b)$ (e Å^{-3})	$\nabla^2\rho(\mathbf{r}_b)$ (e Å^{-5})	ε	$G(\mathbf{r}_b)$ (h Å^{-3})	$H(\mathbf{r}_b)$ (h Å^{-3})
C1—C4	1.5319 (9)	1.63 (3)	−9.96 (5)	0.04	1.35	−2.05
		1.691	*−14.395*	*0.05*	*0.367*	*−1.37*
C2—C3	1.5223 (9)	1.71 (2)	−11.14 (4)	0.07	1.44	−2.22
		1.747	*−15.366*	*0.06*	*0.381*	*−1.46*
C3—C5	1.5382 (10)	1.64 (2)	−9.39 (4)	0.04	1.40	−2.05
		1.679	*−14.099*	*0.03*	*0.395*	*−1.38*
C5—C6	1.5278 (11)	1.65 (2)	−9.62 (4)	0.07	1.40	−2.07
		1.667	*−13.791*	*0.00*	*0.384*	*−1.35*
C5—C7	1.5308 (11)	1.59 (2)	−8.49 (4)	0.06	1.34	−1.93
		1.651	*−13.506*	*0.01*	*0.387*	*−1.33*
C1—N1	1.4922 (9)	1.66 (2)	−7.78 (6)	0.03	1.51	−2.06
		1.689	*−14.863*	*0.03*	*0.680*	*−1.72*
C2—N1	1.4810 (9)	1.71 (2)	−8.53 (6)	0.08	1.57	−2.17
		1.719	*−15.800*	*0.05*	*0.731*	*−1.84*
C4—N1	1.4856 (9)	1.68 (2)	−7.36 (6)	0.02	1.57	−2.09
		1.711	*−15.484*	*0.04*	*0.711*	*−1.79*
C3—O1	1.4473 (9)	1.61 (3)	−4.23 (9)	0.09	1.58	−1.88
		1.588	*−9.536*	*0.04*	*1.526*	*−2.19*
H3···H4b^{i}	2.111	0.071 (5)	0.903 (2)	0.25	0.05	0.01
		0.061	*0.875*	*0.17*	*0.047*	*0.01*
H10···O100	1.901	0.14 (2)	2.78 (2)	0.05	0.16	0.03
N100—O100	1.2557 (8)	3.02 (3)	−3.06 (6)	0.16	4.93	−5.15
P1—F1	1.6077 (12)	1.26 (1)	−1.69 (8)	0.30	1.11	−1.22
P1—F2	1.6147 (13)	1.21 (1)	0.04 (8)	0.33	1.11	−1.11

1987), although a plot of the scale factor *versus* sin θ/λ shows no discernable trend at the highest angles.

DFT(B3LYP) UHF–SCF calculations were carried out on the open-shell cationic complex in (1) using the *GAMESS-UK* program (Guest *et al.*, 2002), with a triplet ground-state configuration for Ni^{2+}, and using the experimentally derived geometry. The size of the problem precludes an all-electron calculation with an extensive basis on all atomic centres. As a compromise, we have performed calculations with triple ξ bases for the N and O atoms (6-311G**), double ξ for Ni (Wachters+f) and a 6-31G** basis for the remaining C/H atoms (EMSL, 2004). A set of natural spin-free orbitals was generated from the UHF wavefunction and these were then used to compute the atomic properties using a locally modified version of the *AIMPAC* programs (Biegler-König *et al.*, 1982) or *AIM*2000 (Biegler-König, 2000).

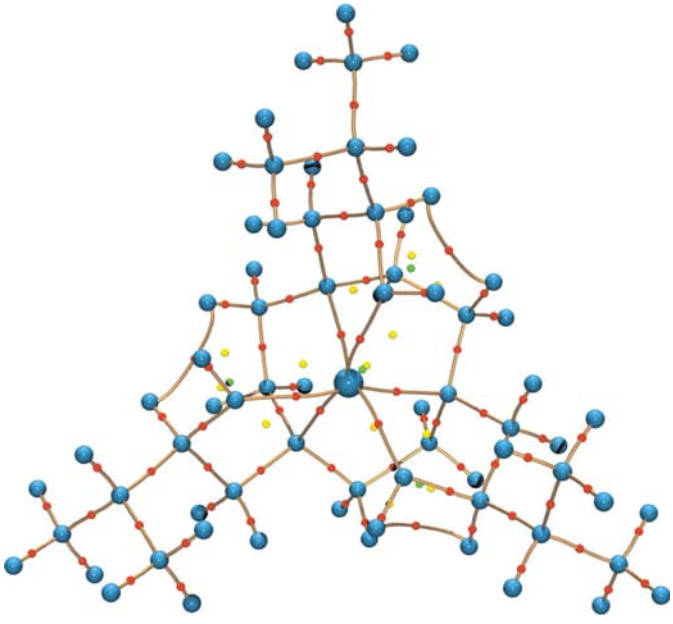

Figure 2
Molecular graph of the cation of (1) from the experimental study. Atomic centres are shown as blue spheres and CPs as small spheres. The colour coding for CPs is red (3,−1), yellow (3,+1) and green (3,+3).

3. Results and discussion

3.1. The H_3L ligand

The critical-point (CP) data in $\rho(\mathbf{r}_b)$, relating to the macrocyclic ligand H_3L, are given in Table 2, and the full molecular graph tracing all the bond paths for the cation is shown in Fig. 2. All the expected bond-critical points (BCPs) were observed for the covalent bonds. Ring CPs were found for the backbone of the TACN (1,4,7-triazacyclononane) ring, and for all six of the five-membered chelate rings linking the Ni centre. A cage CP near the TACN ring CP was also observed. Each of the H···H interactions (see below) generates a new BCP, two ring CPs and a cage CP (as required to satisfy the Poincaré–Hopf rule), all of which were located. The theoretical molecular graph is essentially identical. The values of $\rho(\mathbf{r}_b)$ in Table 2 are uniformly smaller and the values of $\nabla^2\rho(\mathbf{r}_b)$ uniformly less negative than those we originally reported (Smith *et al.*, 1997). Nevertheless, the internal agreement is good and the values are close to those typically expected (Koritsanszky & Coppens, 2001) for single C—C, C—N and C—O covalent bonds. Agreement with the theoretical values of $\rho(\mathbf{r}_b)$ is excellent, while for $\nabla^2\rho(\mathbf{r}_b)$ it is only qualitative, possibly due to the limited basis set used for the C atoms in the DFT calculations. The kinetic energy densities $G(\mathbf{r}_b)$ for the experimental data given in Table 2 have been estimated using a functional approximation (Abramov, 1997) and the total energy densities $H(\mathbf{r}_b)$ calculated from the potential energy densities using the local virial relationship (Bader, 1990). While this function (Abramov, 1997) provides a good approximation for $G(\mathbf{r})$ in regions far from the nuclear centres (where the Laplacian $\nabla^2\rho(\mathbf{r})$ is positive), it is a much poorer approximation close to the nuclei or in regions of local charge concentration where $\nabla^2\rho(\mathbf{r})$ is negative, and only gives qualitative results in these cases (Gálvez *et al.*, 2001).

An interesting aspect of the topology of the H_3L ligand in (1), which was not noticed in our previous studies, is the presence of weak intramolecular (sp_3)CH···HC(sp_3) interac-

Table 3
Properties at the (3,−3) CPs in $-\nabla^2\rho(\mathbf{r})$ in the VSCC of N1.

CP	r (Å)	$\rho(\mathbf{r})$ (e Å^{-3})	$\nabla^2\rho(\mathbf{r})$ (e Å^{-5})
CP(1) ⇒ C1	0.410	3.33	−51.9
CP(2) ⇒ C2	0.409	3.37	−51.2
CP(3) ⇒ C4	0.410	3.33	−48.6
CP(4) ⇒ Ni1	0.405	3.50	−59.3

Table 4
Properties at the (3,−3) CPs in $-\nabla^2\rho(\mathbf{r})$ in the VSCC of O1.

CP	r (Å)	$\rho(\mathbf{r})$ (e Å^{-3})	$\nabla^2\rho(\mathbf{r})$ (e Å^{-5})
CP(1) ⇒ C3	0.347	5.98	−115.6
CP(2) ⇒ H10	0.346	6.16	−126.2
CP(3) ⇒ Ni1	0.348	5.76	−110.7

tion involving H3···H4b^{i}. This closed-shell interaction between a methine and methylene group involves H atoms that bear similar charges. Bader and coworkers (Matta *et al.*, 2003) have recently suggested that these types of dihydrogen interactions should be distinguished from the more common AH···HB dihydrogen bonds (Custelcean & Jackson, 2001; Popelier, 1998; Alkorta *et al.*, 2002; Grabowski, 2001) that have a strong electrostatic component. Similar weak CH···HC interactions have been observed in experimental charge-density studies on 1,3,5,7-tetra-*tert*-butyl-*s*-indacene (Wang *et al.*, 2004) and in tetraphenylborate salts of guanidinium and biguanidinium salts (Robertson *et al.*, 2003). The H3···H4b^{i} interaction in (1), with associated curved bond path and high ellipticity, is detected in both the experimental and theoretical charge densities, and with similar topological properties which are given in Table 2. The H3···H4b^{i} distance of 2.111 Å is a relatively short contact, although it is not the shortest intramolecular H···H contact. Discounting those contacts incapable of generating a bond path (*i.e.* internal CH_2 and CH_3 contacts), the shortest is H2a···H6b = 2.097 Å. Neither this latter contact nor any of the other intramolecular H···H contacts under 2.3 Å generate a BCP and hence a bond path in the experimental density. However, dependent on the basis set, a bond path may be observed between H2a···H6b in the theoretical density. This basis-set dependent topological element is nevertheless structurally unstable. The density is very flat at the BCP and there is a ring CP situated only 0.066 Å away, which differs in density by only 1.9×10^{-5} e Å^{-3}. Moreover, the two CPs have λ_2 values which are, within uncertainty, very close to zero (± 0.026 e Å^{-5}). In addition to this weak H···H interaction, there is also a bond path generated for the 'normal' hydrogen-bonding interaction between the alcohol OH proton and the O atom of the nitrate anion, H10···O100 = 1.901 Å, O1—H10···O100 = 157.1°. The topological properties of this hydrogen bond (Table 2) are typical (Koch & Popelier, 1995; Espinosa *et al.*, 1998; Espinosa, Lecomte & Molins, 1999; Espinosa, Souhassou, Lachekar & Lecomte, 1999; Espinosa *et al.*, 2001; Macchi *et al.*, 2000).

The disposition of the critical points in $L(\mathbf{r}) \equiv -\nabla^2\rho(\mathbf{r})$ in the valence-shell charge concentration (VSCC), *i.e.* the atomic graphs, for the ligator atoms N1 and O1 are shown in Fig. 3, and the CP data are given in Tables 3 and 4. The (3,−3) CPs may be associated with the formal Lewis bonding pairs and lone pairs (Bader, 1990). The N1 atom shows four such CPs arranged in an approximately tetrahedral arrangement, associated with the three covalent bonds to C1, C2 and C4, and the formal dative bond to Ni1. This graph is topologically identical to that of the C atom in CH_4 (Bader, 1990) and is fully consistent with a tetrahedral 'sp^3 hybridized' N atom acting as a σ donor. A similar situation was observed (Iversen *et al.*, 1997) for the N atom of the ammonia ligand in *trans*-$[Ni(NH_3)_4(NO_2)_2]$. On the other hand, the atomic graph of the O1 atom is more interesting, showing only three (3,−3) CPs arranged in a trigonal arrangement that is virtually co-planar with the O atom. This is different from the atomic graph of the O atom in water [which also shows four 'tetrahedral' (3,−3) CPs; Bader, 1990], but is more consistent with an 'sp^2 hybridized' O atom, formally with an unhybridized p-orbital orthogonal to the CP plane (such as found for the C atom of formaldehyde; Bader, 1990). As we noted previously (Smith *et al.*, 1997), the (3,−3) CP associated with the O—Ni bond is that closest to the bond vectors, thus potentially maximizing any π donor interaction. However, the evidence for a Ni—O π interaction is rather ambiguous. The bonding geometry around O1 is distinctly pyramidal and the ellipticity of the Ni—O bonds (see below) is not consistent with any significant Ni—O π interaction.

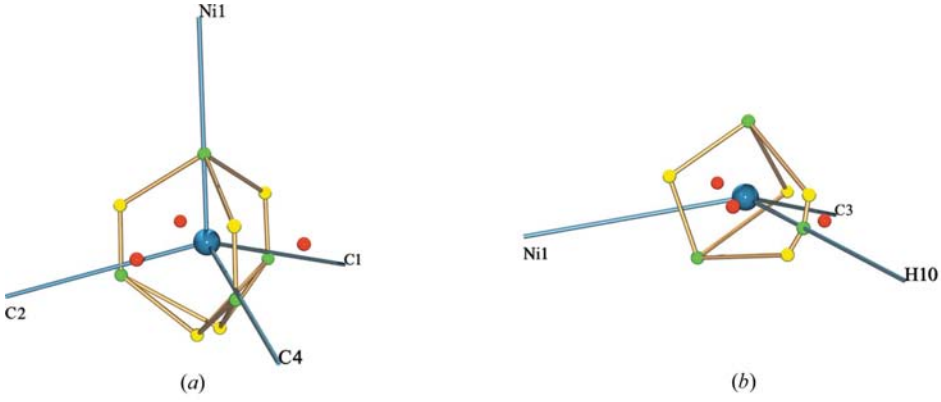

Figure 3
Experimental atomic graphs of (*a*) the N1 atom and (*b*) the O1 atom in (1) showing the CPs in $L(\mathbf{r}) \simeq -\nabla^2\rho(\mathbf{r})$ in the VSCC. Colour coding for the CPs is (3,−3) green, (3,−1) yellow and (3,+1) red. The blue lines show the bond vectors, not the bond paths.

3.2. The nickel ion

As discussed in §2, the Ni atom was treated somewhat differently than in our original report. The P_v monopole population is 8.42 (4), *i.e.* slightly greater than previously obtained, but since we use a neutral atom-scattering factor

Table 5
Symmetry-adapted *d*-orbital populations.

Orbital	Experiment	Crystal field	DFT
a_1 (d_{z^2})	1.82 (2)	2.0	1.98
e ($d_{x^2-y^2}$, d_{xy})	3.43 (2)	4.0	3.46
e (d_{xz}, d_{yz})	3.16 (2)	2.0	2.81

(with a formal 4*s* population of 2.0) rather than a doubly charged ion, the resultant formal charge on Ni is −0.42 compared with a previous formal charge of +0.90. The overall *d*-orbital population may be decomposed (Holladay *et al.*, 1983) into symmetry-adapted *d*-orbital populations, which are given in Table 5. Under C_3 symmetry, the five *d*-orbitals transform as a_1, *e* and *e*. The populations are in the order expected from simple crystal-field theory, except that the high-lying *e* set is more populated and the lower a_1 and *e* sets are less populated than predicted. This is consistent with appreciable covalency. Mulliken population analysis on the DFT natural orbital wavefunction gives a total *d*-orbital population of 8.25, with individual populations in reasonable agreement with experiment. An alternative method of determining atomic charges is to partition the electron population within the atomic basins defined by the zero-flux surfaces (Bader, 1990). The experimental AIM integrated charges on the Ni, O and N atoms are +0.50 (+1.20), −1.14 (−1.10) and −0.85 (−0.96), respectively (theoretical values from DFT density in parentheses). The experimental AIM charges are quite dependent on the multipole model. For a model using the Ni^{2+} scattering factor, but otherwise identical, we obtain an integrated charge for the Ni atom of +1.17, *i.e.* very close to the theoretical AIM charge.

The experimental and theoretical Laplacian maps in the Ni1—O1—N1 plane are shown in Fig. 4. The peculiar large lobes of charge concentrations on the Ni centre shown in Figs. 6 and 7 of our original publication (Smith *et al.*, 1997) were due to the scaling error of κ' in *XD*, and are now absent. The atomic graph of the Ni atom (Fig. S2, see supplementary material) is of the form [8,12,6] with eight (3,−3) charge concentrations in $L(\mathbf{r}) \equiv -\nabla^2\rho(\mathbf{r})$ arranged in an approximate cube, 12 (3,−1) saddle CPs along the edges of the cube, and six (3,+1) depletion CPs in the faces of the cube. The Ni atom thus has the cuboidal disposition of charge concentrations that has been experimentally observed in many octahedrally (or pseudo-octahedrally) coordinated transition metals (Abramov *et al.*, 1998; Hwang & Wang, 1998; Lee *et al.*, 2002; Macchi & Sironi, 2003; Farrugia *et al.*, 2003; Farrugia & Evans, 2005). The eight charge concentrations on the Ni atom maximally avoid the ligand charge concentrations, as expected from simple ligand-field theory. The six charge concentrations on the ligator N and O atoms align with the six charge depletions on the Ni atom, as is evident from Fig. 4. This is an example of the 'lock and key' concept (Bader, 1990; Koritsanszky & Coppens, 2001; Macchi & Sironi, 2003; Cortés-Guzman & Bader, 2005) in coordination complexes. The atomic graph of Ni shows the same topology in both the experimental and theoretical densities, but in the former the charge concentration lying along the threefold axis in the direction of N1 and its three associated (3,−1) saddle points are only 0.012 Å apart. The theoretical graph does not show this C_3 distortion and is very close to ideal O_h symmetry.

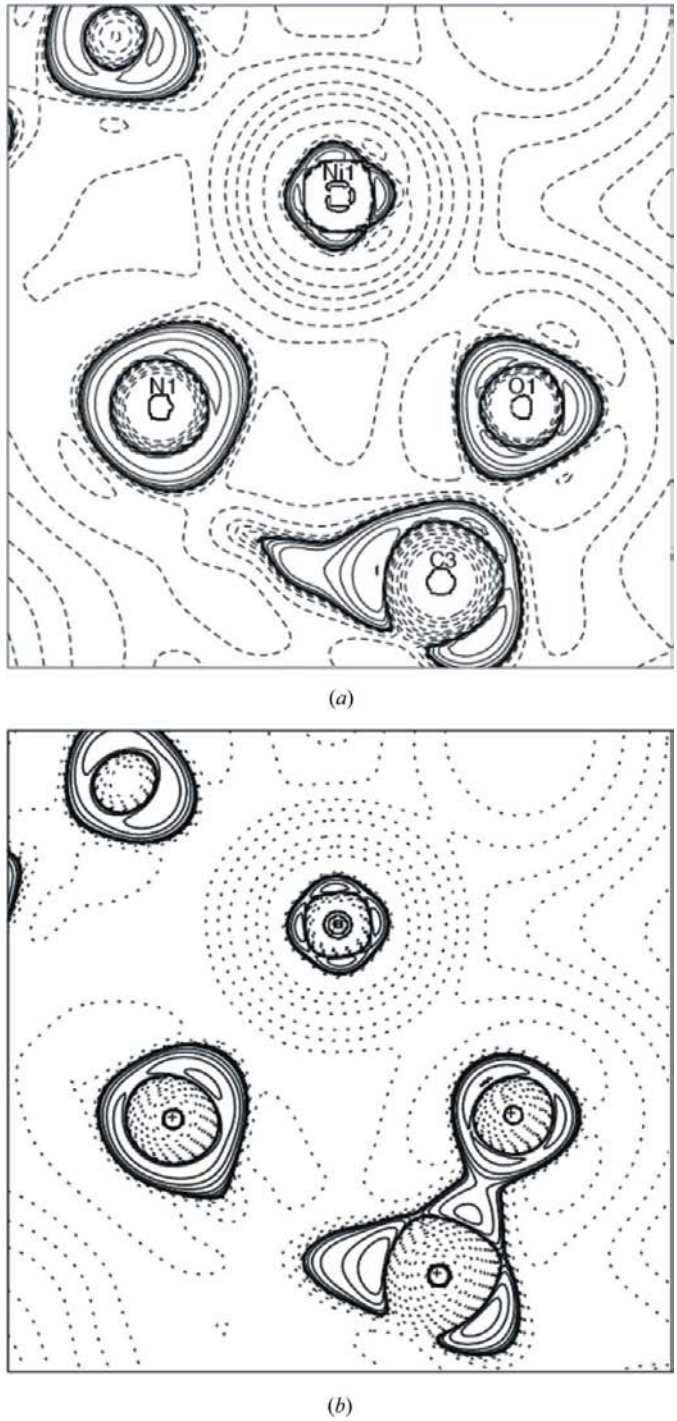

Figure 4
Laplacian distribution $L(\mathbf{r}) \simeq -\nabla^2\rho(\mathbf{r})$ in the N1—O1—Ni1 plane: (*a*) from the experimental study and (*b*) from the DFT calculation on the $[Ni(L_3H)]^{2+}$ cation. Contours are drawn at -1.0×10^{-3}, $\pm 2.0 \times 10^n$, $\pm 4 \times 10^n$, $\pm 8 \times 10^n$ (n = −3, −2, −1, 0, +1, +2) e Å^{-5}, with positive contours drawn with a full line and negative contours with a broken line.

Table 6
BCP properties for the metal–ligand bonds.

R_{ij} is the length of the bond path, r_j are the distances along the bond path of the BCP from the second atom. The first line gives the experimental values and the second line the theoretical values.

Bond	Length (Å)	R_{ij} (Å)	r_j (Å)	$\rho(\mathbf{r}_b)$ (e Å^{-3})	$\nabla^2\rho(\mathbf{r}_b)$ (e Å^{-5})	ε	$G(\mathbf{r}_b)$ (h Å^{-3})	$H(\mathbf{r}_b)$ (h Å^{-3})
Ni1—N1	2.0633 (7)	2.073	1.080	0.550 (5)	8.836 (5)	0.16	0.71	−0.09
		2.066	*1.094*	*0.532*	*8.647*	*0.13*	*0.69*	*−0.09*
Ni1—O1	2.0935 (7)	2.124	1.090	0.418 (3)	7.057 (4)	0.20	0.52	−0.02
		2.103	*1.088*	*0.387*	*8.014*	*0.17*	*0.57*	*−0.01*

3.3. Topological properties of the metal–ligand bonds

The CP data for the nickel–ligand bonds are given in Table 6. The values of $\rho(\mathbf{r}_b)$ are substantially smaller, especially for Ni1—N1, than those we originally reported (Smith *et al.*, 1997) and compare well with the theoretical values. One crucial difference between the current and original interpretations lies in the position of the BCP, which is significantly shifted towards the midpoint of the Ni–X vector, thus reducing the magnitude of $\rho(\mathbf{r})$. The value of $\nabla^2\rho(\mathbf{r}_b)$ and the ellipticities ε are similar for the two bonds. A significant Ni—O π interaction would be expected to lead to a larger ellipticity than is observed, so any Ni—O π-bonding must be quite minor. This is consistent with chemical intuition, since the low-lying a and e levels of the Ni^{2+} cation (corresponding to the t_{2g} d-orbital level of an octahedral complex) are formally filled and are therefore incapable of accepting π-density from the (potentially) π-donating O atom.

Another particularly unusual feature in our original report (Smith *et al.*, 1997) was the trifurcated and highly curved bond path, which left the Ni atom towards the three ligating O atoms. This 'feature' has been commented on in a recent review (Koritsanszky & Coppens, 2001), but again we find this to be an artefact due to the programming errors in *XD*. The molecular graph in Fig. 2 shows a much more expected situation, with six bond paths associated with the six Ni–ligand bonds. The bond paths leave the Ni atom approximately along the octahedral axes and are reasonably straight, being only slightly longer than the direct internuclear vectors (see Table 6).

The positive values of $\nabla^2\rho(\mathbf{r}_b)$ for the Ni—N and Ni—O bonds are now well established as typical of bonds to transition metals. Within the dichotomous classification (Bader & Essén, 1984), these would be indicative of closed-shell or ionic bonding. However, it has been clear for some time that this simple classification is inadequate to describe bonding to transition metals (Koritsanszky & Coppens, 2001; Macchi & Sironi, 2003; Cortés-Guzman & Bader, 2005; Gatti, 2005). Indeed, in our original study (Smith *et al.*, 1997) we noted that 'it would appear that the topological properties of covalent metal–ligand bonds do not have the same characteristics as covalent bonding between first-row atoms'. It has been suggested (Macchi & Sironi, 2003) that in order to fully characterize a chemical bond, a number of topological criteria need to be examined, rather than merely the magnitudes and/or sign of $\rho(\mathbf{r}_b)$ and $\nabla^2\rho(\mathbf{r}_b)$. These criteria include the topology of $\nabla^2\rho(\mathbf{r})$ along the bond path, the delocalization indices $\delta(A,B)$ (Fradera *et al.*, 1999), the local energy densities $H(\mathbf{r}_b)$ (Cremer & Kraka, 1984) or $N(A,B) = \oint_{A\cap B}\rho(\mathbf{r})$, the integrated density (Cremer & Kraka, 1984) over the zero-flux surface shared by the two atoms. Other authors (Marabello *et al.*, 2004; Gervasio *et al.*, 2004) have suggested an extension of the dichotomous classification involving a transit zone for bonds to transition metals.

While delocalization indices $\delta(A,B)$ are very useful indicators of chemical bonding, they are unfortunately not easily computable for the open-shell case. The spin populations obtained from the DFT wavefunction are suggestive of some shared interactions, with the percentage locations of the two unpaired electrons being Ni, 79.6%; N, 5.0%; O, 1.45%. The values of $\rho(\mathbf{r}_b)$ for the Ni—N and Ni—O bonds may be compared with other recent studies on nickel(II) complexes, *e.g.* for *trans*-$[Ni(NH_3)_4(NO_2)_2]$, Ni—N = 0.65 (2), 0.76 (2) e Å^{-3} (Iversen *et al.*, 1997); for $[Ni(C_4N_4H_2)_2]$, Ni—N = 0.94 e Å^{-3} (Hwang & Wang, 1998); $[Ni(C_4O_4)(OH_2)_4]$, Ni—O = 0.44, 0.47 e Å^{-3} (Lee *et al.*, 1999); and a square-planar nickel(II) Schiff base complex, Ni—O = 0.581 (5), Ni—N = 0.522 (5), 0.644 (6), 0.711 (6) e Å^{-3} (Kožíšek *et al.*, 2004). Our values of $\rho(\mathbf{r}_b)$ are at the lower end of these, but are sufficiently large to suggest a significant shared interaction. On the other hand, $G(\mathbf{r}_b)/\rho(\mathbf{r}_b)$ for both bonds is greater than 1.0 and $H(\mathbf{r}_b)$ is only very slightly negative, suggesting a significant ionic component.

While $\rho(\mathbf{r}_b)$ has been shown to be a useful indicator of bond order for strong covalent bonds (Bader *et al.*, 1982), in the case of transition metal–ligand bonding, which potentially involves the very diffuse 4*s* orbitals, it may be more useful to compare $N(A,B) = \oint_{A\cap B}\rho(\mathbf{r})$, the integrated density over the interatomic surface. Values for $N(A,B)$ for the Ni—N and Ni—O bonds of 1.02 and 0.87 e Å^{-1}, respectively, were obtained from a DFT wavefunction with 6-31G** bases on all centres (at the HF level these values were $\sim$10% smaller). These are somewhat smaller than the typical value of $\sim$2 e Å^{-1} found for the strongly covalent M—C bonds in transition metal carbonyls (Macchi & Sironi, 2003; Farrugia *et al.*, 2003), but are significantly larger than values for classic ionic interactions, *e.g.* 0.46 e Å^{-1} for NaF (Macchi & Sironi, 2003). A profile of $\nabla^2\rho(\mathbf{r})$ along the internuclear vectors (Fig. 5) shows that the Laplacian at the BCP is dominated by the large charge

concentrations of the ligator atoms, especially so for the Ni—N bond. The profiles most closely resemble that for Na—F (Macchi & Sironi, 2003).

4. Conclusions

This reappraisal of the charge density in (1) shows that several of the unusual features that were originally reported (Smith *et al.*, 1997) are in fact artefacts due to coding errors in the early version of *XD* used. The topological properties of the newly obtained experimental charge density compare well with theoretical densities obtained from DFT(B3LYP) UHF–SCF calculations. Taken together, these topological indicators point to significantly less of a shared interaction for the Ni–N and Ni–O bonds than found for example in metal–carbonyl bonds. If it is profitable to translate the topological characteristics into classical chemical terms like covalent or ionic, we may say that the Ni—N and Ni—O bonds are 'intermediate' cases that have some definite covalent character, albeit with a strong ionic component that is more pronounced for the Ni—O bond. Although the alcohol O atom has an atomic graph that is more consistent with sp^2 hybridization, and thus 'set up' for Ni—O π-bonding, there is no convincing experimental evidence for much π-character in this bond. These conclusions are in accordance with chemical intuition.

We thank the EPSRC for support (GR/F 77852, GR/J 22702) and for a postgraduate studentship for GTS.

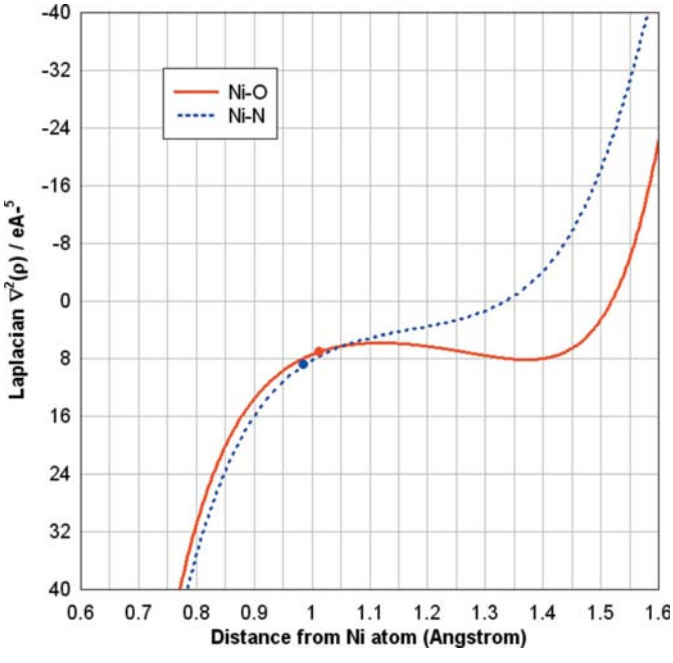

Figure 5
Profile of the experimental Laplacian $\nabla^2\rho(\mathbf{r}_b)$, in the region of the BCPs for the Ni—N and Ni—O bonds. The filled circles mark the positions of the BCPs.

References

Abramov, Y. A. (1997). *Acta Cryst.* A**53**, 264–272.
Abramov, Y. A., Brammer, L., Klooster, W. T. & Bullock, R. M. (1998). *Inorg. Chem.* **37**, 6317–6328.
Alkorta, I., Elguero, J., Mó, O., Yáñez, M. & Del Bene, J. E. (2002). *J. Phys. Chem. A*, **106**, 9325–9330.
Bader, R. F. W. (1990). *Atoms in Molecules: A Quantum Theory.* Oxford University Press.
Bader, R. F. W. & Essén, H. (1984). *J. Chem. Phys.* **80**, 1943–1960.
Bader, R. F. W., Tang, T.-H., Tal, Y. & Biegler-König, F. W. (1982). *J. Am. Chem. Soc.* **104**, 946–952.
Biegler-König, F. (2000). *J. Comput. Chem.* **21**, 1040–1048.
Biegler-König, F. W., Bader, R. F. W. & Tang, T.-H. (1982). *J. Comput. Chem.* **3**, 317–328.
Blessing, R. H. (1987). *Cryst. Rev.* **1**, 3–58.
Bunge, C. F., Barrientos, J. A. & Bunge, A. V. (1993). *At. Data Nucl. Data Tables*, **53**, 113–162.
Cortés-Guzman, F. & Bader R. F. W. (2005). *Coord. Chem. Rev.* **249**, 633–662.
Cremer, D. & Kraka, E. (1984). *Croat. Chem. Acta*, **57**, 1259–1281.
Custelcean, R. & Jackson, J. E. (2001). *Chem. Rev.* **101**, 1963–1980.
Destro, R. & Marsh, R. E. (1987). *Acta Cryst.* A**43**, 711–718.
El Haouzi, A., Hansen, N. K., Le Hénaff, C. & Protas, J. (1996). *Acta Cryst.* A**52**, 291–301.
EMSL (2004). Basis sets were obtained from the Extensible Computational Chemistry Environment Basis Set Database, Version 02/25/04, as developed and distributed by the Molecular Science Computing Facility, Environmental and Molecular Sciences Laboratory, which is part of the Pacific Northwest Laboratory, PO Box 999, Richland, Washington 99352, USA, and funded by the US Department of Energy. The Pacific Northwest Laboratory is a multi-program laboratory operated by the Battelle Memorial Institute for the US Department of Energy under contract DE-AC06-76RLO 1830. Contact David Feller or Karen Schuchardt for further information.
Enraf–Nonius (1994). *CAD*-4. Enraf–Nonius, Delft, The Netherlands.
Espinosa, E., Alkorta, I., Rozas, I., Elguero, J. & Molins, E. (2001). *Chem. Phys. Lett.* **336**, 457–461.
Espinosa, E., Lecomte, C. & Molins, E. (1999). *Chem. Phys. Lett.* **300**, 745–748.
Espinosa, E., Molins, E. & Lecomte, C. (1998). *Chem. Phys. Lett.* **285**, 170–173.
Espinosa, E., Souhassou, M., Lachekar, H. & Lecomte, C. (1999). *Acta Cryst.* B**55**, 563–572.
Fallis, I. A., Farrugia, L. J., Macdonald, N. M. & Peacock, R. D. (1993). *J. Chem. Soc. Dalton Trans.* pp. 2759–2763.
Farrugia, L. J. (1997). *J. Appl. Cryst.* **30**, 565–566.
Farrugia, L. J. & Evans, C. (2005). *C. R. Chim.* **8**, 1566–1583.
Farrugia, L., Mallinson, P. R. & Stewart, B. (2003). *Acta Cryst.* B**59**, 234–247.
Fradera, X., Austen, M. A. & Bader, R. F. W. (1999). *J. Phys Chem. A*, **103**, 304–314.
Gálvez, O., Gómez, P. C. & Pacios, L. F. (2001). *Chem. Phys. Lett.* **337**, 263–268.
Gatti, C. (2005). *Acta Cryst.* A**61**, C47–C48.
Gervasio, G., Bianchi, R. & Marabello, D. (2004). *Chem. Phys. Lett.* **387**, 481–484.
Grabowski, S. J. (2001). *J. Phys. Chem. A*, **105**, 10739–10746.
Guest, M. F., Kendrick, J., van Lenthe, J. H. & Sherwood, P. (2002). *GAMESS-UK*, Version 6.3. The DFT module within GAMESS-UK was developed by Dr P. Young under the auspices of EPSRC's Collaborative Computational Project No. 1 (CCP1, 1995–1997).
Hansen, N. K. & Coppens, P. (1978). *Acta Cryst.* A**34**, 909–921.
Hirshfeld, F. L. (1976). *Acta Cryst.* A**32**, 239–244.
Holladay, A., Leung, P. & Coppens, P. (1983). *Acta Cryst.* A**39**, 377–387.
Hwang, T.-S. & Wang, Y. (1998). *J. Phys. Chem. A*, **102**, 3726–3731.

Iversen, B. B., Larsen, F. K., Figgis, B. N. & Reynolds, P. A. (1997). *J. Chem. Soc. Dalton Trans.* pp. 2227–2240.
Koch, U. & Popelier, P. L. A. (1995). *J. Phys. Chem.* **99**, 9747–9754.
Koritsanszky, T. & Coppens, P. (2001). *Chem. Rev.* **101**, 1583–1627.
Koritsanszky, T., Howard, S. T., Mallinson, P. R., Su, Z., Richter, T. & Hansen, N. K. (1995). *XD*. Freie University, Berlin, Germany.
Koritsanszky, T., Howard, S. T., Richter, T., Macchi, P., Volkov, A., Gatti, C., Mallinson, P. R., Farrugia, L. J., Su, Z. & Hansen, N. K. (2003). *XD*. Freie University, Berlin, Germany.
Kožíšek, J., Fronc, M., Skubák, P., Popkov, A., Breza, M., Fuess, H. & Paulmann, C. (2004). *Acta Cryst.* A**60**, 510–516.
Lee, C.-R., Wang, C.-C., Chen, K.-C., Lee, G.-H. & Wang, Y. (1999). *J. Phys. Chem. A*, **103**, 156–165.
Lee, J.-J., Lee, G.-H. & Wang, Y. (2002). *Chem. Eur. J.* **8**, 1821–1832.
Macchi, P., Garlaschelli, L. & Sironi, A. (2002). *J. Am. Chem. Soc.* **124**, 14173–14184.
Macchi, P., Iversen, B. B., Sironi, A., Chakoumakos, B. C. & Larsen, F. K. (2000). *Angew. Chem. Int. Ed.* **39**, 2719–2722.
Macchi, P., Proserpio, D. & Sironi, A. (1998). *J. Am. Chem. Soc.* **120**, 1447–1455. A corrected version of one of the figures has been posted on the Internet at http://dcssi.istm.cnr.it/Macchi/nicod.htm.
Macchi, P., Schultz, A. J., Larsen, F. K. & Iversen, B. B. (2001). *J. Chem. Phys. A*, **105**, 9231–9242.
Macchi, P. & Sironi, A. (2003). *Chem. Rev.* **238**, 383–412.
Marabello, D., Bianchi, R., Gervasio, G. & Cargnoni, F. (2004). *Acta Cryst.* A**60**, 494–501.
Matta, C., Hernández-Trujillo, J., Tang, T.-H. & Bader, R. F. W. (2003). *Chem. Eur. J.* **9**, 1940–1951.
Pérès, N., Boukhris, A., Souhassou, M., Gavoille, G. & Lecomte, C. (1999). *Acta Cryst.* A**55**, 1038–1048.
Popelier, P. L. A. (1998). *J. Chem. Phys. A*, **102**, 1873–1878.
Ptasiewicz-Bak, H., Olovsson, I. & McIntyre, G. J. (1999). *Acta Cryst.* B**55**, 830–840.
Robertson, K. N., Knop, O. & Cameron, T. S. (2003). *Can. J. Chem.* **81**, 727–743.
Su, Z. & Coppens, P. (1998). *Acta Cryst.* A**54**, 646–652.
Scherer, W. & McGrady, G. S. (2004). *Angew. Chem. Int. Ed. Engl.* **43**, 1782–1806.
Sheldrick, G. M. (1993). *SHELXS*93. University of Göttingen, Germany.
Smith, G. T., Mallinson, P. R., Frampton, C. S., Farrugia, L. J., Peacock, R. D. & Howard, J. A. K. (1997). *J. Am. Chem. Soc.* **119**, 5028–5034.
Smith, G. T., Mallinson, P. R., Peacock, R. D., Farrugia, L. J., Fallis, I. A., Frampton, C. S. & Howard, J. A. K. (1996). *J. Chem. Soc. Chem. Commun.* pp. 525–526.
Tafipolsky, M., Scherer, W., Öfele, K., Artus, G., Pedersen, B., Herrmann, W. A. & McGrady, G. S. (2002). *J. Am. Chem. Soc.* **124**, 5865–5880.
Wang, C.-C., Tang, T.-H., Wu, L.-C. & Wang, Y. (2004). *Acta Cryst.* A**60**, 488–493.